BIOMOLECULES & THERAPEUTICS

Original Article
Biomol Ther 29(1), 41-51 (2021)

KF-1607, a Novel Pan Src Kinase Inhibitor, Attenuates Obstruction-Induced Tubulointerstitial Fibrosis in Mice

Debra Dorotea[1], Seungyeon Lee[2], Sun Joo Lee[2], Gayoung Lee[1], Jung Beom Son[2], Hwan Geun Choi[2], Sung-Min Ahn[3,4,5] and Hunjoo Ha[1,*]

[1]Graduate School of Pharmaceutical Sciences, College of Pharmacy, Ewha Womans University, Seoul 03760,
[2]New Drug Development Center, Daegu-Gyeongbuk Medical Innovation Foundation, Daegu 41061,
[3]Department of Genome Medicine and Science, College of Medicine, Gachon University, Seongnam 13120,
[4]Department of Hematology-Oncology, Gachon University Gil Hospital, Incheon 21565,
[5]ImmunoForge, Seoul 08826, Republic of Korea

Abstract

Src family kinases (SFKs), an important group of non-receptor tyrosine kinases, are suggested to be excessively activated during various types of tissue fibrosis. The present study investigated the effect of KF-1607, an orally active and a newly synthesized Src kinase inhibitor (SKI) with proposed low toxicity, in preventing the progression of renal interstitial fibrosis. Unilateral ureteral obstruction (UUO) surgery was performed in 6-week-old male C57BL/6 mice to induce renal interstitial fibrosis. Either KF-1607 (30 mg/kg, oral gavage) or PP2 (2 mg/kg, intraperitoneal injection), a common experimental SKI, was administered to mice for seven days, started one day prior to surgery. UUO injury-induced SFK expression, including Src, Fyn, and Lyn kinase. SFK inhibition by KF-1607 prevented the progression of tubular injury in UUO mice, as indicated by decreases in albuminuria, urinary KIM-1 excretion, and kidney NGAL protein expression. Renal tubulointerstitial fibrosis was attenuated in response to KF-1607, as shown by decreases in α-SMA, collagen I and IV protein expression, along with reduced Masson's trichrome and collagen-I staining in kidneys. KF-1607 also inhibited inflammation in the UUO kidney, as exhibited by reductions in F4/80 positive-staining and protein expression of p-NFκB and ICAM. Importantly, the observed effects of KF-1607 were similar to those of PP2. A new pan Src kinase inhibitor, KF-1607, is a potential pharmaceutical agent to prevent the progression of renal interstitial fibrosis.

Key Words: Src kinase, Src kinase inhibitor, Ureteral obstruction, Renal fibrosis, Chronic kidney disease

INTRODUCTION

Chronic kidney disease (CKD) is an emerging worldwide health problem and imposes a high risk of cardiovascular complications (De Nicola and Zoccali, 2016; Hill *et al*., 2016; Zhou and Liu, 2016a). To date, only a few therapeutic options are clinically utilized to prevent CKD progression, particularly for renin-angiotensin system blockers (Ruggenenti *et al*., 2012). However, high CKD prevalence implies that current therapies cannot adequately prevent and/or reverse renal fibrosis, the common final outcome leading to permanent renal parenchyma loss and progressive renal function decline (Wynn and Ramalingam, 2012; Breyer and Susztak, 2016). Therefore, it remains imperative to find a more effective agent to halt CKD progression.

Src family kinases (SFKs) are a family of proto-oncogenic non-receptor tyrosine kinases. To date, nine members of the Src family have been identified: c-Src, Fyn, Yes, Lyn, Fgr, Hck, Blk, Lck, and Yrk kinases. Src, Fyn, Yes, and Yrk kinases are ubiquitously expressed, whereas the others are found primarily in hematopoietic cells. The activated kinases phosphorylate specific tyrosine residues of signal transducers, such as AKT and STAT3. Under normal physiological conditions, they regulate various biological activities including cell survival, proliferation, and migration (Boggon and Eck, 2004; Parsons and Parsons, 2004). In contrast, aberrant SFK activity is classically implicated in tumor cell adhesion, migration, invasion, and metastasis (Thomas and Brugge, 1997).

Excessive Src kinase activation stimulates fibroblast activation and enhanced extracellular matrix (ECM) accumulation in

Open Access **https://doi.org/10.4062/biomolther.2020.088**

Received May 18, 2020 **Revised** Jun 2, 2020 **Accepted** Jun 4, 2020
Published Online Jul 21, 2020

***Corresponding Author**
E-mail: hha@ewha.ac.kr
Tel: +82-2-3277-3001, Fax: +82-2-3277-2851

systemic sclerosis and bleomycin-induced lung fibrosis models (Skhirtladze *et al*., 2008; Hu *et al*., 2014). Various extracellular cues, such as transforming growth factor (TGF)-β1, angiotensin II, epidermal growth factor, and ECM can also activate Src kinases. Src activation induces phosphorylation of signaling proteins which amplifies multiple fibrogenic signaling pathways (Zhou and Liu, 2016b). Although information on which isoform(s) of the SFKs are predominantly activated under specific kidney disease states is lacking, various experimental models of both acute and chronic kidney disease have reported higher Src kinase expression as compared to basal conditions. Correspondingly, Src kinase inhibition by experimental pan inhibitors, such as PP1 and PP2, demonstrated a protective effect against kidney injuries (Taniguchi *et al*., 2013; Wu *et al*., 2015; Yan *et al*., 2016; Xiong *et al*., 2017).

Current FDA-approved pan-Src kinase inhibitors (SKIs), such as dasatinib, bosutinib, and ponatinib, are mainly used for treatment of chronic myelogenous leukemia (Drake *et al*., 2014). However, fewer studies have investigated efficacy of these pan-Src inhibitors in chronic diseases, such as metabolic disorders and fibrosis. In the present study, the expression of SFK members was observed in mice with unilateral ureteral obstruction (UUO) injury, an experimental model of CKD. Using this model, the pharmacological effects of KF-1607, a newly synthesized and orally active SKI, was assessed and compared with PP2, a common experimental SKI used in several preclinical tissue fibrosis studies.

MATERIALS AND METHODS

Chemicals and reagents

All chemicals were obtained from Sigma-Aldrich (St. Louis, MO, USA), unless otherwise stated.

Synthesis of KF-1607

^{1}H NMR experiments were achieved using an Avance III 400 MHz NMR spectrometer equipped with a 5-mm broadband observed probe head (Bruker, Billerica, MA, USA). The NMR spectrum optimization was conducted using Bruker Topspin 3.1 software (Bruker), and all parameters were set in the program. The compounds were dissolved in dimethyl sulfoxide (DMSO)-d_6 and the spectra were acquired at 25°C. Mass spectra were measured in positive electrospray ionization mode on an LCMS-2020 system (Shimadzu, Tokyo, Japan). Column chromatography was performed using a Combi-Flash Rf system with RediSep Rf (Teledyne Isco, Lincoln, NE, USA). Analytical HPLC was performed on a YMC-Park Pro C18, 150×4.6 mm column using gradient conditions (5-100% B over nine minutes, flow rate=1.0 mL min^{-1}). The eluents used were solvent A (H_2O with 0.1% trifluoroacetic acid [TFA]) and solvent B (acetonitrile, CH_3CN). Reagents and solvents were purchased and used without further purification.

Synthesis of sec-butyl 3-((8-chloroimidazo[1,2-a]pyridin-3-yl)ethynyl)-4-methylbenzoate (Supplementary Fig. 1)

8-chloro-3-iodoimidazo[1,2-a]pyridine (2): To a solution of 8-chloroimidazo[1,2-a]pyridine (1, 20 g, 131 mmol) in dimethylformamide (DMF; 150 mL) was added N-iodosuccinimide (35.4 g, 157 mmol) at –10°C. After 0.5 h, the reaction mixture was warmed to room temperature and stirred for 1 h. After completion of the reaction, the mixture was washed with ice-water. The resulting precipitate was collected by filtration and dried to give the title compound (2) as a dark brown solid (35.0 g, 96% yield). The crude product was used for the next step without further purification. ^{1}H NMR (400 MHz, DMSO-*d6*) δ 8.34 (d, *J*=6.8 Hz, 1H), 7.78 (s, 1 H), 7.55 (d, *J*=7.0 Hz, 1H), 7.05 (t, *J*=7.1 Hz, 1H); MS *m/z* : 279 $[M+H]^+$.

8-chloro-3-((trimethylsilyl)ethynyl)imidazo[1,2-a]pyridine (3): To a solution of 8-chloro-3-iodoimidazo[1,2-a]pyridine (2, 35.0 g, 126 mmol) in CH_3CN (30 mL) were added ethynyltrimethylsilane (11.6 mL, 84.0 mmol), tetrakis (triphenylphosphine)palladium(0) ($Pd(PPh_3)_4$; 4.84 g, 4.19 mmol), copper iodide (CuI; 1.60 g, 8.38 mmol), and diisopropylethylamine (DIPEA; 24.8 mL, 142 mmol) at room temperature. The reaction mixture was warmed to 80°C and stirred for 1 h. After completion of the reaction, the mixture was cooled to room temperature and filtered through a pad of celite. The filtrate was concentrated in a vacuum. The residue was diluted with ethyl acetate (c) and washed with brine. The organic layer was dried over with sodium sulfate (Na_2SO_4) and then concentrated. The crude product was purified by silica gel column chromatography (hexane [Hex]: dichloromethane [DCM]=3:1 to Hex:DCM=1:9) to give the title compound (3) as a brown solid (19.0 g, 91% yield).

^{1}H NMR (400 MHz, DMSO-*d6*) δ 8.40 (dd, *J*=6.7, 0.8 Hz, 1H), 8.01 (s, 1 H), 7.62 (dd, *J*=7.4, 0.8 Hz, 1H), 7.12 (t, *J*=7.1 Hz, 1H), 0.30 (s, 9H); MS *m/z* : 249 $[M+H]^+$.

8-chloro-3-ethynylimidazo[1,2-a]pyridine (4): To a solution of 8-chloro-3-((trimethylsilyl)ethynyl)imidazo[1,2-a]pyridine (3, 19.0 g, 76.0 mmol) in tetrahydrofuran (THF; 100 mL) was added potassium carbonate (K_2CO_3; 52.8 g, 382 mmol) at room temperature. The reaction mixture was added to methanol (MeOH; 100 mL) and stirred for 0.5 h. After completion of the reaction, the resulting mixture was filtered through a pad of celite and then vacuum-concentrated. The residue was added into water and stirred at room temperature for 0.5 h. The resulting precipitate was washed with water, filtered and dried to give the title compound (4) as a yellow solid (13.0 g, 96% yield).

^{1}H NMR (400 MHz, DMSO-*d6*) δ 8.46 (dd, *J*=6.8, 0.8 Hz, 1H), 8.01 (s, 1 H), 7.61 (dd, *J*=7.4, 0.6 Hz, 1H), 7.09 (t, *J*=7.1 Hz, 1H), 5.16 (s, 1H); MS *m/z* : 177 $[M+H]^+$.

sec-butyl 3-((8-chloroimidazo[1,2-a]pyridin-3-yl)ethynyl)-4-methylbenzoate (5): To a solution of 8-chloro-3-ethynylimidazo[1,2-a]pyridine (4, 15.0 g, 85.0 mmol) in DMF (100 mL) were added sec-butyl 3-iodo-4-methylbenzoate (27.0 g, 85.0 mmol), DIPEA (22.2 mL, 127 mmol), CuI (1.62 g, 8.49 mmol), and $Pd(PPh_3)_4$ (4.91 g, 4.25 mmol) at room temperature. The reaction mixture was warmed to 100°C and stirred for 16 h. After completion of the reaction, the resulting mixture was cooled to room temperature, filtered through a pad of celite and co-evaporated with toluene. The residue was purified by silica gel column chromatography (Hex: EtOAc=2:8) to give the title compound (5) as a yellow solid (25.0 g, 80% yield).

^{1}H NMR (400 MHz, DMSO-*d6*) δ 8.64 (dd, *J*=6.7, 0.8 Hz, 1H), 8.15 (d, *J*=1.8 Hz, 1H), 8.13 (s, 1H), 7.90 (dd, *J*=8.0, 1.8 Hz, 1H), 7.65 (dd, *J*=7.4, 0.8 Hz, 1H), 7.53 (d, *J*=8.1 Hz, 1H), 7.15 (t, *J*=7.1 Hz, 1H), 2.59 (s, 3H), 1.76-1.60 (m, 2H), 1.30 (d, *J*=6.3 Hz, 3H), 0.92 (t, *J*=7.4 Hz, 1H); MS *m/z* : 367 $[M+H]^+$.

Synthesis of 4-methyl-3-((8-((1-(piperidin-4-yl)-1H-pyrazol-4-yl)amino) imidazo[1,2-a]pyridin-3-yl)ethynyl)-N-(3-(trifluoromethyl)phenyl)benzamide Hydrochloride salt (10) (Supplementary Fig. 2)

3-((8-chloroimidazo[1,2-a]pyridin-3-yl)ethynyl)-4-methylbenzoic acid (6): To a solution of *sec*-butyl 3-((8-chloroimidazo[1,2-a]pyridin-3-yl)ethynyl)-4-methylbenzoate (5, 2.50 g, 6.81 mmol) in THF/MeOH/water (6 mL/4 mL/4 mL) was added lithium hydroxide (LiOH; 0.490 g, 20.4 mmol) at room temperature. The reaction mixture was warmed to 60°C and stirred for 3 h. After completion of the reaction, the resulting mixture was cooled to room temperature. The reaction mixture was acidified with 1N HCl and stirred for 0.5 h. The resulting precipitate was collected by filtration and dried to give the title compound (6) as a yellow solid (1.90 g, 90% yield).

^{1}H NMR (400 MHz, DMSO-*d6*) δ 8.65 (dd, *J*=6.7, 0.8 Hz, 1H), 8.17 (d, *J*=1.7 Hz, 1H), 8.12 (s, 1H), 7.89 (dd, *J*=7.9, 1.8 Hz, 1H), 7.65 (dd, *J*=7.4, 0.8 Hz, 1H), 7.50 (d, *J*=8.0 Hz, 1H), 2.58 (s, 3H); MS *m/z* : 311 $[M+H]^+$.

3-((8-chloroimidazo[1,2-a]pyridin-3-yl)ethynyl)-4-methyl-N-(3-(trifluoromethyl)phenyl) ben-zamide (7): To a solution of 3-((8-chloroimidazo[1,2-a]pyridin-3-yl)ethynyl)-4-methylbenzoic acid (6, 1.90 g, 6.11 mmol) in DMF (10 mL) were added 3-(trifluoromethyl)aniline (1.08 g, 6.73 mmol), 1-ethyl-3-(3-dimethylaminopropyl)carbodiimide (1.76 g, 9.17 mmol) and N,N-dimethylpyridin-4-amine (1.12 g, 9.17 mmol) at room temperature. The reaction mixture was stirred at 60°C for 8 h. After completion of the reaction, the resulting mixture was cooled to room temperature, extracted with DCM and washed by brine. The combined organic layer was dried over Na_2SO_4 and concentrated. The residue was purified by silica gel column chromatography (DCM: MeOH=9:1) to give the title compound (7) as a pale brown solid (2.20 g, 79% yield).

^{1}H NMR (400 MHz, DMSO-*d6*) δ 10.61 (br s, 1H), 8.63 (d, *J*=6.6 Hz, 1H), 8.27 (d, *J*=9.7 Hz, 2H), 8.13 (s, 1H), 8.08 (d, *J*=7.5 Hz, 1H), 7.95 (d, *J*=6.5 Hz, 1H), 7.68-7.53 (m, 3H), 7.47 (d, *J*=7.2 Hz, 1H), 7.17 (t, *J*=7.0 Hz, 1H), 2.61 (s, 3H); MS *m/z* : 454 $[M+H]^+$.

tert-butyl 4-(4-((3-((2-methyl-5-((3-(trifluoromethyl)phenyl)carbamoyl)phenyl)ethynyl) imidazo [1,2-a]pyridin-8-yl) amino)-1H-pyrazol-1-yl)piperidine-1-carboxylate (8): To a solution of 3-((8-chloroimidazo[1,2-a]pyridin-3-yl)ethynyl)-4-methyl-N-(3-(trifluoromethyl) phenyl)benzamide (7; 600 mg, 1.32 mmol) in t-butanol (BuOH; 5.0 mL) were added tert-butyl 4-(4-amino-1H-pyrazol-1-yl)piperidine-1-carboxylate (387 mg, 1.45 mmol), cesium carbonate (Cs_2CO_3; 1,292 g, 3.97 mmol) at room temperature and then heated to 80°C. The mixture was degassed under N_2 for 10 min and then XPhos Pd G2 (104 mg, 0.132 mmol) was added to the mixture at 80°C. The reaction mixture was stirred at 130°C for 20 h. After completion of the reaction, the resulting mixture was cooled to 80°C, and then hot-filtered through a pad of celite and concentrated. The residue was purified by silica gel column chromatography (DCM: MeOH=9:1) to give the title compound (8) as a brown solid (200 mg, 22% yield).

^{1}H NMR (400 MHz, DMSO-*d6*) δ 10.61 (br s, 1H), 8.28-8.22 (m, 3H), 8.08 (d, *J*=8.0 Hz, 1H), 7.98 (s, 1H), 7.96-7.91 (m, 3H), 7.62 (t, *J*=8.3 Hz, 1H), 7.56-7.53 (m, 2H), 7.47 (d, *J*=7.6 Hz, 1H), 6.98 (t, *J*=7.1 Hz, 1H), 6.63 (d, *J*=7.5 Hz, 1H), 4.37-4.28 (m, 1H), 4.09-4.01 (m, 2H), 2.99-2.82 (m, 2H), 2.61 (s, 3H), 2.04-1.98 (m, 2H), 1.88-1.76 (m, 2H), 1.42 (s, 9H); MS *m/z* : 684 $[M+H]^+$.

4-methyl-3-((8-((1-(piperidin-4-yl)-1H-pyrazol-4-yl)amino) imidazo[1,2-a]pyridin-3-yl)ethynyl)-N-(3-(trifluoromethyl) phenyl)benzamide (9): To a solution of tert-butyl 4-(4-((3-((2-methyl-5-((3-(trifluoromethyl)phenyl)carbamoyl)phenyl) ethynyl)imidazo[1,2-a]pyridin-8-yl)amino)-1H-pyrazol-1-yl) piperidine-1-carboxylate (8, 200 mg, 0.293 mmol) in DCM (2 mL) was added TFA (1.0 mL, 13.1 mmol) at room temperature. The reaction mixture was stirred at room temperature for 1 h. After completion of the reaction, the resulting mixture was concentrated under reduced pressure. The TFA salt was neutralized with saturated sodium bicarbonate ($NaHCO_3$) (aqueous) for 1 h. The residue was extracted three times with DCM and then the combined organic layer was washed with water, dried over Na_2SO_4 and concentrated. The residue was purified by silica gel column chromatography (DCM: MeOH=7:3) to give the title compound (9) as a pale-yellow solid (187 mg, 92% yield).

^{1}H NMR (400 MHz, DMSO-*d6*) δ 10.62 (br s, 1H), 8.27-8.24 (m, 2H), 8.22 (s, 1H), 8.08 (d, *J*=8.2 Hz, 1H), 7.98 (s, 1H), 7.96-7.91 (m, 2H), 7.88 (s, 1H), 7.61 (t, *J*=8.0 Hz, 1H), 7.57-7.53 (m, 2H), 7.47 (d, *J*=7.7 Hz, 1H), 6.98 (t, *J*=7.1 Hz, 1H), 6.61 (d, *J*=7.5 Hz, 1H), 4.24-4.13 (m, 1H), 3.11-3.03 (m, 2H), 2.68-2.57 (m, 5H), 2.01-1.92 (m, 2H), 1.88-1.76 (m, 2H); MS *m/z* : 584 $[M+H]^+$.

4-methyl-3-((8-((1-(piperidin-4-yl)-1H-pyrazol-4-yl)amino) imidazo[1,2-a]pyridin-3-yl)ethynyl)-N-(3-(trifluoromethyl) phenyl)benzamide Hydrochloride salt (10): To a solution of 4-methyl-3-((8-((1-(piperidin-4-yl)-1H-pyrazol-4-yl)amino) imidazo[1,2-a]pyridin-3-yl)ethynyl)-N-(3-(trifluoromethyl)phenyl)benzamide (9, 187 mg, 0.320 mmol) in acetone (4 mL) was added HCl (4N in dioxane, 0.801 mL, 3.20 mmol) at room temperature and then stirred for 1 h. Diethyl ether was added into the mixture, and then the mixture was stirred for 1 h. The resulting precipitate was collected by filtration and dried to produce the title compound (10) as a beige solid (180 mg, 91% yield).

^{1}H NMR (400 MHz, DMSO) δ 10.75 (s, 1H), 9.24-9.16 (m, 1H), 9.07 (br s, 1H), 9.01-8.89 (m, 1H), 8.56 (s, 1H), 8.38 (d, *J*=1.7 Hz, 1H), 8.30 (s, 1H), 8.25 (d, *J*=6.4 Hz, 1H), 8.12 (d, *J*=8.4 Hz, 1H), 8.01 (dd, *J*=8.0, 1.8 Hz, 1H), 7.98 (s, 1H), 7.63 (s, 1H), 7.61-7.54 (m, 2H), 7.46 (d, *J*=7.8 Hz, 1H), 7.34-7.27 (m, 1H), 7.02 (d, *J*=7.9 Hz, 1H), 4.57-4.46 (m, 1H), 3.82-3.65 (m, 2H), 3.21-3.01 (m, 2H), 2.61 (s, 3H), 2.28-2.12 (m, 4H); ^{13}C NMR (101 MHz, DMSO) δ 164.79, 143.72, 139.94, 133.87, 133.28, 133.15, 132.32, 131.11, 130.18, 129.95, 129.54, 129.22, 129.10, 125.58, 123.93, 122.87, 121.78, 121.74, 120.97, 120.10, 118.33, 116.50, 115.21, 109.59, 97.76, 79.03, 55.45, 42.13, 28.61, 20.60; MS *m/z* : 584 $[M+H]^+$; purity: 99.4% (HPLC t_R 5.64 min).

Kinase assay

The enzyme activities of SFKs were determined by Reaction Biology Corporation (Malvern, PA, USA), using 10 concentrations in a 3-fold dilution series of KF-1607 starting at 10 μM.

Kinetic measurement of cytotoxicity

Mouse mesangial cells, SV40 MES 13, were purchased from American Type Culture Collection (Manassas, VA, USA), and maintained in Dulbecco's Modified Eagle Medium low glucose (Gibco, Grand Island, NY, USA) supplemented with 10% fetal bovine serum (Gibco), at 37°C in humidified 5%

CO_2. SV40 MES 13 cells at a density of 1×10^3 cells per well were plated in 96-well plates overnight. The medium was then replaced with fresh medium containing the indicated concentrations of KF-1607 and 50 nM of the YOYO-1 cytotoxicity reagent (Essen Biosciences, Ann Arbor, MI, USA), a fluorescent, cell-impermeant cyanine dimer, nucleic acid-staining dye. When added to culture media, YOYO-1 fluorescently stains nuclear DNA of cells that have lost plasma membrane integrity. YOYO-1 fluorescence was monitored over 48 h and quantified according to the manufacturer's instructions.

In vivo animal experiments

All animal experiments were approved by the Institutional Animal Care and Use Committee of Ewha Womans University (IACUC No. 16-066). Unilateral ureteral obstruction (UUO) surgery was performed in 6-week-old male C57BL/6 mice (Central Lab Animal Inc., Seoul, Korea) as described in our previous study (Lee *et al*., 2013). Mice were anesthetized with Zoletil (0.006 mL per 10 g, Virbac, Seoul, Korea)/ Rompun (0.004 mL per 10 g, Bayer, Ansan, Korea). Anesthetized mice were placed on a heating pad set at 37°C. Following a flank incision, the left ureter was ligated with silk (4/0) at two locations and was cut between these ligations. Sham-operated mice underwent the same surgical procedure except for the ureter ligation and cut. Following surgical site closure, mice were monitored until fully recovered. The UUO mice were treated with either KF-1607 or PP2 (1-(tert-butyl)-3-(4-chlorophenyl)-1H-pyrazolo[3,4-d]pyrimidin-4-amine) (Calbiochem, San Diego, CA, USA). Based on our preliminary study, KF-1607 was administered orally 30 mg/kg per day. PP2 was administered 2 mg/kg per day via intraperitoneal injection as suggested by the previous studies (Taniguchi *et al*., 2013; Wu *et al*., 2015). Drug administration was started at one day prior to UUO surgery, and mice were euthanized after 7 days of drug treatment.

Measurement of urine parameters

Prior to necropsy, urine samples were collected in a metabolic cage for 24 h and centrifuged at 3,000 rpm for 10 min. Urinary albumin excretion and kidney injury molecule-1 (KIM-1) were measured by ELISA kits, provided by ALPCO (Westlake, OH, USA) and R&D Systems (Minneapolis, MN, USA), respectively.

Measurement of lipid peroxide (LPO)

Before necropsy, blood samples were collected using a heparinized syringe. Blood samples were centrifuged at 3,000 rpm for 15 min at 4°C, and plasma was collected for lipid peroxide (LPO) measurements. Plasma and urine concentrations of LPO were measured as thiobarbituric acid reactive substances according to the literature (Ha *et al*., 1999). Briefly, aliquots were mixed with 8% sodium dodecyl sulfate and a mixture containing 0.8% 2-thiobarbituric acid and 20% acetic acid. This solution was kept at 95°C for 60 min. After stopping the reaction by cooling it down, the mixtures were centrifuged at 4,000 rpm for 5 min to precipitate interfering particulate materials. The amount of LPO was then measured spectrofluorometrically. While, the LPO concentration in the kidney was measured using an LPO assay kit (Cayman Chemical, Ann Arbor, MI, USA) according to the manufacturer's protocol.

Histology and immunohistochemical staining

Kidneys were fixed with 2% paraformaldehyde-lysine-periodate (pH 7.4), dehydrated, and embedded in paraffin. Kidney tissue sections (5 μm) were stained with Masson's trichrome stain to detect matrix collagen accumulation. The tissue sections were also immuno-stained overnight at 4°C with primary antibodies, i.e., anti-F4/80 (Santa Cruz Biotechnology, CA, USA) and anti-collagen I (Southern Biotech, Birmingham, AL, USA). Briefly, the tissue sections were de-paraffinized and successively incubated in 3% hydrogen peroxide and 5% normal goat serum, avidin/biotin blocking solution (Vector Laboratories, Burlingame, CA, USA), primary antibody, and specific secondary antibody (Vector Laboratories). Bound antibodies were visualized with 3,3-diaminobenzidine (DAB; Dako, Glostrup, Denmark). Images were obtained using a Zeiss microscope equipped with an Axio Cam HRC digital camera and Axio Cam software (Zeiss, Thornwood, NY, USA) and quantified with Image-Pro Plus4.5 software (Cybernetics, Silver Spring, MD, USA).

Immunoblot analysis

Protein concentrations of kidney tissue homogenate were determined using Bradford methods (BioRad Laboratories, Hercules, CA, USA). Proteins were separated by electrophoresis and subsequently transferred onto a PVDF membrane (GE Healthcare BioSciences Co., Piscataway, NJ, USA). Membranes were blocked with 5% skim milk in TBS-Tween 20 buffer for 1 h at room temperature. Immunoblots were incubated at 4°C in a 1:1,000 dilution of the indicated antibodies as follows: anti-p-Fyn, anti-Fyn, anti-GAPDH, anti-ICAM, and anti-Lyn (Santa Cruz Biotechnology); anti-p-NFκB, anti-p-Src, and anti-Src, (Cell Signaling Technology, Danvers, MA, USA); anti-collagen I and anti-collagen IV (Southern Biotech); anti-α-SMA (Abcam, Cambridge, MA, USA); anti-NGAL (Ab-Frontier, Seoul, Korea); and anti-p-Lyn (Bioss, Woburn, MA, USA). Positive immunoreactive bands were detected using an enhanced chemiluminescence method (LAS-3000, FUJIFILM Corporation, Tokyo, Japan). Densitometer analysis of immu-

Table 1. Mouse primer sequence used in the present study

Gene	Forward primer (5'-3')	Reverse primer (5'-3')
18S	CGA AAGCAT TTGCCAAGA AT	AGT CGGCATCGTTTATGG TC
Src	TCCACACCTCTCCGAAGCAA	CATGCTGATGGCCTGTGTCA
Fyn	CTTTGGGGGTGTGAACTCCT	TTCTGCCTGGATGGAGTCAA
Lyn	AGCTCCAGAGGCCATCAACT	CACATCTGCGTTGGTTCTCC
Hck	TCCCACATCCACCATCAAGC	TCTTCGTGGTGAATGGCCTC
Lck	ACGATCTCGGGGATCATGG	GAGATCTTGCTGTCCAGTGGG
Yes	TGGGAATCAGCGAGGTATTT	ACATTGTCACCCCTCACCTC

noblot results is presented as the ratio between target protein and GAPDH.

Real-time PCR

Total cellular RNA was extracted using TRIzol reagent (Invitrogen, Carlsbad, CA, USA). Real-time PCR was performed using ABI7300 (Applied Biosystems, Carlsbad, CA, USA) with a 20 μL reaction volume consisting of cDNA transcripts, primer pairs, and SYBR Green PCR Master Mix (Applied Biosystems). The mouse-specific primer sequences are listed in Table 1. 18S RNA was used as an internal control to normalize the genes.

Bioinformatics analysis

The Expression Atlas at the European Bioinformatics Institute (EMBL-EBI) (http: //www.ebi.ac.uk/gxa) was utilized to explore the baseline expression of SFKs in mouse and human kidneys. Baseline data sets are sourced from selected, high-quality RNA-seq data sets, and gene expression quantification values are expressed in TPM (transcripts per million) units (Papatheodorou *et al*., 2018). In addition, the transcriptomics data were all provided by the Nephroseq database (http://nephroseq.org) and were re-analyzed to identify gene expression in a selected renal disease and to integrate these data with clinical data (Papadopoulos *et al*., 2016). The *Neusser Hypertension Glom* dataset exhibits gene expression profiling of 18 micro-dissected glomeruli samples, which were analyzed on an Affymetrix human U133A GeneChip platform of which four were controls and 14 were nephrosclerosis samples (Neusser *et al*., 2010). The *Flechner Transplant* dataset was utilized to analyze the correlation between a specific SFK member with a chosen clinical parameter. In this study, gene expression from kidney biopsy samples (n=31) taken from kidney transplant patients or normal healthy controls was measured using Affymetrix HG-U95Av2 arrays (Flechner *et al*., 2004).

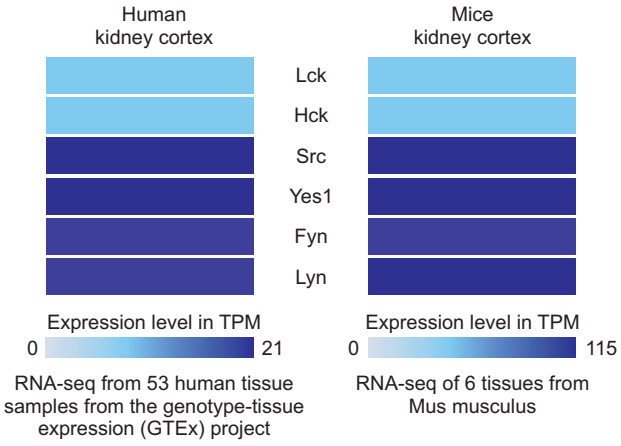

Fig. 1. Baseline expression of SFKs in kidney cortex. RNA-sequencing data of SFKs expression in kidney cortex isolated from control human and mouse samples.

Statistical analysis

All results are expressed as mean ± standard error (SE). Analysis of variance was used to assess differences between multiple groups, followed by Fisher's posthoc analysis. The level of statistical significance was set at *p*-value less than 0.05.

RESULTS

Expression of SFKs in the kidney

As previous studies have not delineated the basal expression of each member of SFKs in the kidney, we initially investigated their expression in both healthy human (*Homo sapiens*) and mouse (*Mus musculus*) samples using Expression Atlas

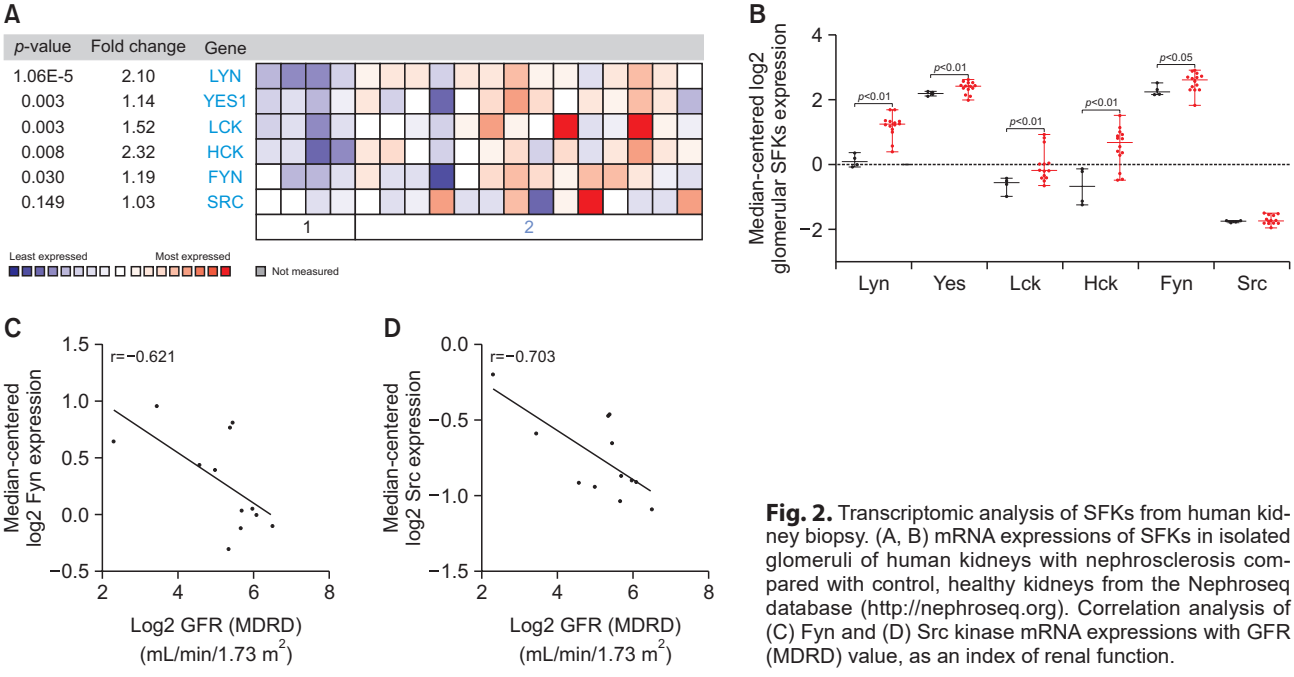

Fig. 2. Transcriptomic analysis of SFKs from human kidney biopsy. (A, B) mRNA expressions of SFKs in isolated glomeruli of human kidneys with nephrosclerosis compared with control, healthy kidneys from the Nephroseq database (http://nephroseq.org). Correlation analysis of (C) Fyn and (D) Src kinase mRNA expressions with GFR (MDRD) value, as an index of renal function.

in the EMBL-EBI database. Src, Fyn, Lyn, Yes, Lck, and Hck kinase were detected in the kidney cortex of both humans and mice with different expression level characteristics. RNA-sequencing analysis revealed that Src kinase was highly expressed, whereas Hck and Lck kinase were least expressed in the kidney cortex (Fig. 1).

To show the significance of SFKs expression in human kidney diseases, transcriptomic analysis of human kidney biopsies provided by the Nephroseq database were explored. Neusser *et al*. (2010) performed gene expression profiling in nephrosclerotic as well as control normal kidney. A diagnosis of nephrosclerosis is based on histological criteria including segmental hyalinosis mainly within the walls of afferent arterioles and sub-endothelial fibrosis of interlobular arteries, as well as focal and segmental glomerulosclerosis and glomerular collapse (Neusser *et al*., 2010). Co-expression analysis from this platform showed that multiple members of SFKs, i.e., Fyn, Lyn, Yes, Hck, and Lck kinases, were significantly over-expressed in fibrotic kidney (Fig. 2A, 2B). The Flechner Transplant Dataset (Flechner *et al*., 2004) further demonstrated that Fyn and Src kinase gene expression was negatively correlated with glomerular filtration rate (GFR) values quantified by the modification of diet in renal disease (MDRD) equation, had a moderate and strong correlations, respectively. Fyn and Src kinases were highly expressed in patients who developed renal dysfunction (Fig. 2C, 2D).

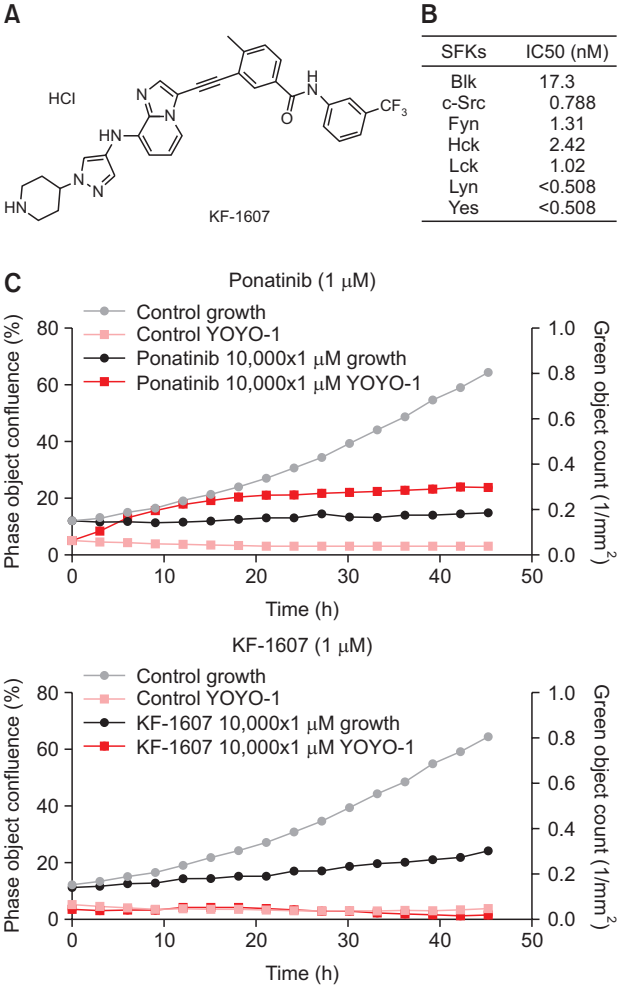

Fig. 3. Characteristics of a newly synthesized SKI, KF-1607. (A) The chemical structure of KF-1607 (4-methyl-3-((8-((1-(piperidin-4-yl)-1H-pyrazol-4-yl)amino) imidazo[1,2-a]pyridin-3-yl)ethynyl)-N-(3-(trifluoromethyl)phenyl)benzamide hydrochloride salt). (B) KF-1607 is a potent pan SKI. (C) Kinetic measurement of cytotoxicity using YOYO®-1 iodide reagent, comparing KF-1607 to ponatinib.

Development of a new SKI

Ponatinib is a highly potent tyrosine kinase inhibitor (TKI) and inhibits not only pan-Bcr-Abl, but also FGFR, PDGFR, VEGFR, RET, FLT3, pan-Src, KIT, TIE2, and EPH receptors at IC_{50}s ranging from 0.1 to 20 nM (O'Hare *et al*., 2009). However, ponatinib exhibited an unexpected wide spectrum of cardiotoxicity which led to its withdrawal from the market in 2013 (Gainor and Chabner, 2015). By maintaining the backbone of ponatinib, a new scaffold with SFKs inhibition properties was created. KF-1607, a next-generation TKI, could be a potential alternative to ponatinib (Fig. 3A). The enzyme activity of KF-1607 was confirmed as nearly similar to that of ponatinib (Fig. 3B). To assess potential toxicity, kinetic evaluation of cytotoxicity was performed using a cell impermeant cyanine dimer nucleic acid stain that binds to dsDNA in a mouse mesangial cell kidney culture. At a similar concentration (1 μM), KF-1607 demonstrated relatively lower toxicity during 40-hours observation in comparison with ponatinib (Fig. 3C).

SFKs are activated following UUO injury in mice

Following UUO injury, the transcript levels of SFK members were analyzed. Compared to sham kidney, Src, Fyn, and Lyn mRNA levels were increased more than 2-fold in UUO kidney (Fig. 4A). Subsequently, we measured the protein expression of these three SFKs. Phosphorylated Src, Lyn, and Fyn kinases were significantly increased in UUO kidney, and were decreased in mice treated with KF-1607 and PP2 (Fig. 4B-4F).

Src kinase inhibition improves kidney function in UUO mice

UUO mice exhibited deterioration of renal function, represented by albuminuria and increased tubular injury, as indicated by urinary KIM-1 and renal NGAL protein expression. Albuminuria was reduced in KF-1607-treated mice (Fig. 5A). Both urinary KIM-1 and NGAL proteins were decreased by both treatments (Fig. 5B-5D).

Src kinase inhibition attenuates progression of tubulointerstitial fibrosis in UUO mice

Tubulointerstitial fibrosis in UUO kidney was described by elevated ECM accumulation detected by Masson's trichrome and collagen-I staining. Both positively-stained areas were significantly reduced by both treatments (Fig. 6A-6C). Consistently, the elevated protein levels of α-SMA, collagen-I, and -IV were decreased in KF-1607 and PP2-treated UUO mice (Fig. 6D-6G).

Src kinase inhibition ameliorates kidney inflammation and oxidative stress in UUO mice

We evaluated macrophage infiltration in the kidney by F4/80 stain. F4/80 positive areas were increased in UUO kidney, which was significantly decreased by both treatments (Fig. 7A, 7B). UUO injury caused increases in protein levels of

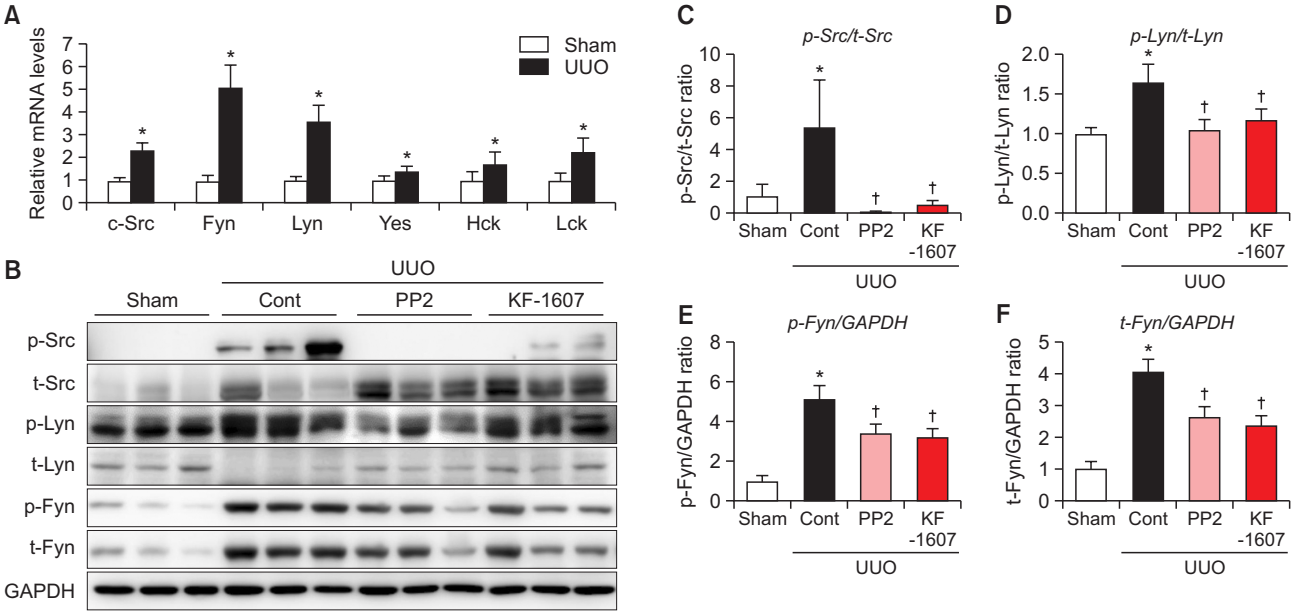

Fig. 4. Expression of SFKs is increased in obstructed kidney as compared to sham kidney. (A) Relative mRNA expressions of SFKs in the kidney of sham and UUO mice. (B) Immunoblotting analysis of phosphorylated- and total- Src, Lyn, and Fyn kinases in the kidney. (C-F) Expression levels of the indicated proteins were quantified by densitometry and normalized with GAPDH. Values are presented as mean ± SE of 6 mice. *p<0.05 vs. sham mice. †p<0.05 vs. UUO control mice.

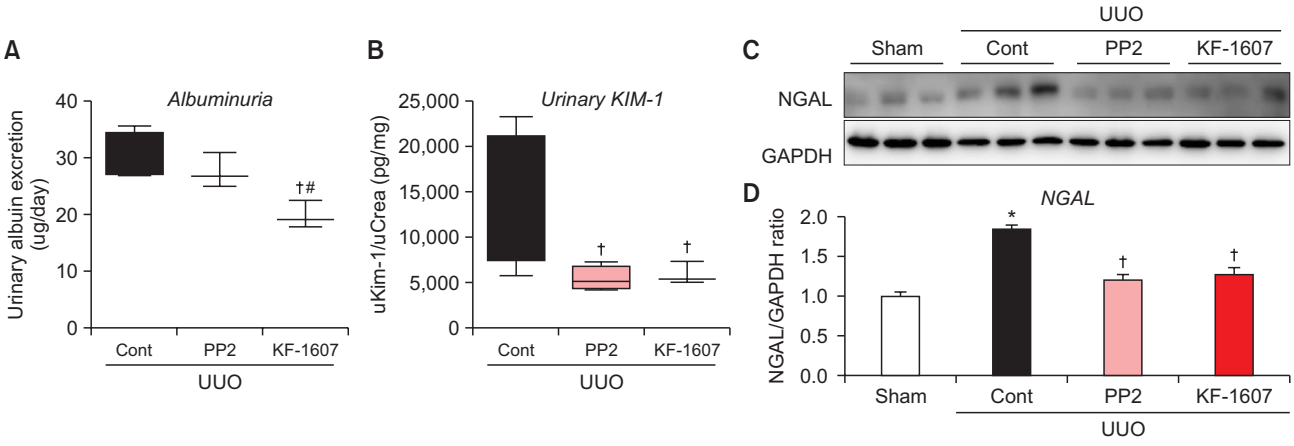

Fig. 5. Src kinase inhibition prevents albuminuria and tubular injury in UUO mice. Urine was analyzed to quantify (A) albumin and (B) KIM-1 levels. (C) Renal NGAL protein expression was analyzed by immunoblotting. (D) Expression levels of the indicated proteins were quantified by densitometry and normalized with GAPDH. Values are presented as mean ± SE of 6 mice. *p<0.05 vs. sham mice. †p<0.05 vs. UUO control mice. #p<0.05 vs. PP2-treated mice.

inflammatory mediators, such as p-NFκB and ICAM. Both proteins were significantly decreased by KF-1607 and PP2 treatments (Fig. 7C-7E). Oxidative stress was analyzed through LPO measurement in plasma, urine, and kidney samples. Increased LPO levels in the plasma and urine were not affected by SKIs treatment (Fig. 8A, 8B); only kidney LPO concentration was significantly decreased in response to KF-1607 treatment (Fig. 8C).

DISCUSSION

KF-1607 is a newly designed and orally active SKI with low toxicity. The present study demonstrated that pan-Src kinase inhibition by KF-1607 prevented the progression of tubular injury in mice with UUO. Accordingly, renal inflammation and tubulointerstitial fibrosis were attenuated in response to KF-1607.

Tyrosine kinases generally have low basal activity and are activated transiently in response to specific stimuli. Most studies have generally focused on the role of Src kinase in kidney pathophysiology, and less is known about the general expres-

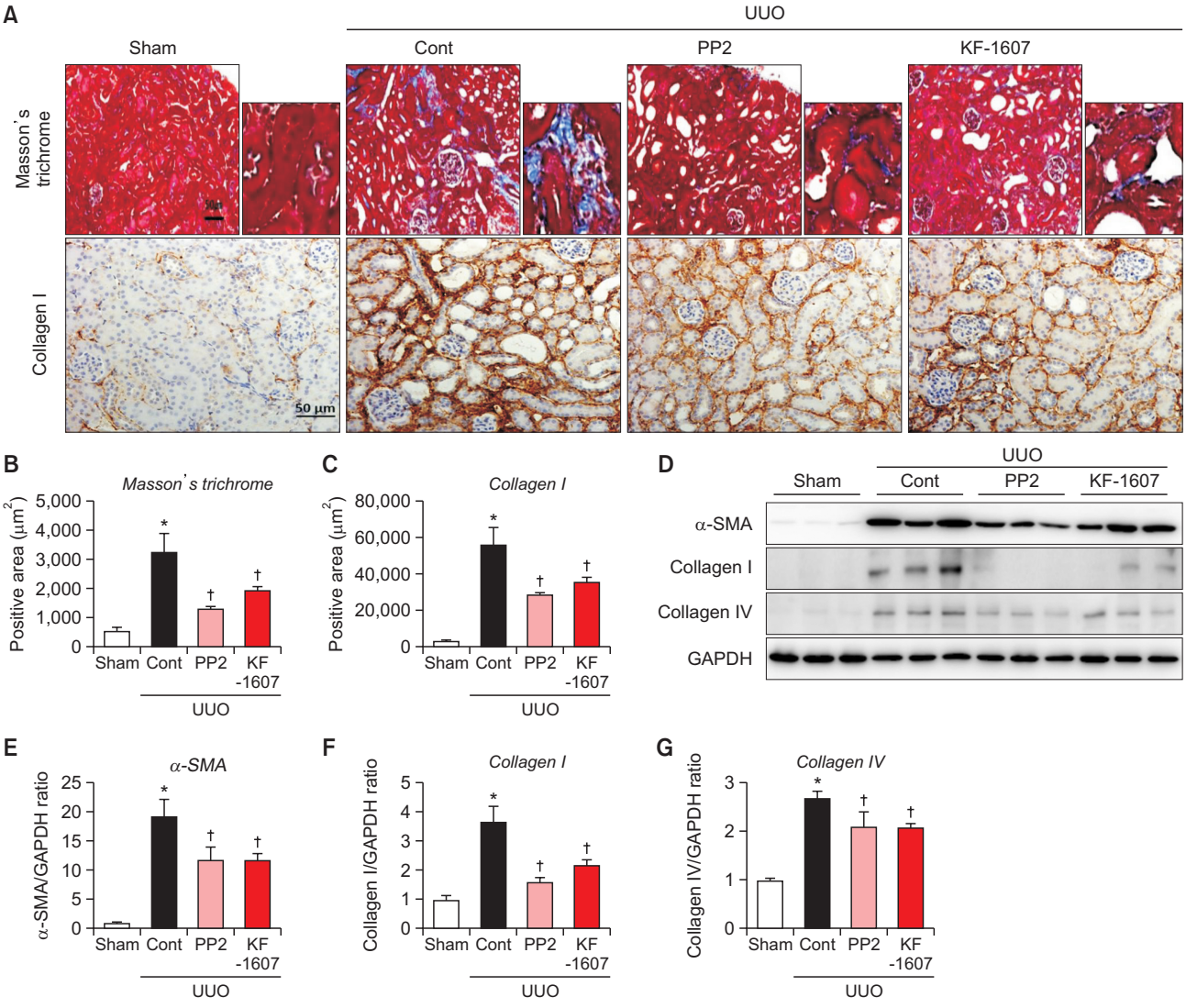

Fig. 6. Src kinase inhibition prevents the progression of tubulointerstitial fibrosis in UUO mice. Representative photomicrographs of (A) Masson trichrome- and collagen I-stained kidney sections. The scale bar indicates 50 μm, original magnification x200. (B, C) Quantitative analysis of positively stained areas in the cortex is depicted. (D) Protein expression of fibrotic markers, α-SMA, collagen I, and collagen IV, were analyzed by immunoblotting. (E-G) Expression levels of the indicated proteins were quantified by densitometry and normalized with GAPDH. Values are presented as mean ± SE of 6 mice. **p*<0.05 vs. sham mice. †*p*<0.05 vs. UUO control mice.

sion of SFK members in the kidney. RNA-sequencing analysis revealed that Src, Lyn, Fyn, and Yes kinases are among the SFKs highly expressed in human and mouse kidney cortex. Among them, Fyn kinase is well-recognized to physiologically maintain the integrity of podocytes by phosphorylating several slit diaphragm components including nephrin, Neph1, and TRPC6 (Hattori *et al*., 2011). Bioinformatics analysis suggests that higher SFK activation is evident in the human kidney during chronic kidney injury. Multiple members of SFKs are elevated in transcriptomic analysis of human kidneys with overt nephrosclerosis (Neusser *et al*., 2010). Interestingly, Fyn and Src kinase genes are overexpressed in patients with renal dysfunction, and exhibit negative correlation with GFR-MDRD (Flechner *et al*., 2004). In addition, the active form of Fyn kinase is increased in patients with obstructive nephropathy (Seo *et al*., 2016). Under our experimental conditions, UUO injury-induced tubulointerstitial fibrosis and SFKs activation. Transcript levels as well as the phosphorylation of Fyn, Lyn, and Src kinase proteins were specifically increased in the kidneys of mice with UUO compared to other isoforms. Among SFK members, Fyn and Src kinases were mostly reported to be activated under chronic kidney injury (Taniguchi *et al*., 2013; Wu *et al*., 2015; Lv *et al*., 2016; Seo *et al*., 2016). However, studies which dissect the exact role of each SFK isoform in mediating tissue fibrosis are limited.

TGF-β1 is a major mediator of ECM protein accumulation in tubulointerstitial fibrosis, and its expression is elevated in renal fibrosis in both human and experimental animal models (Meng *et al*., 2015; Sureshbabu *et al*., 2016). Src induces fibroblast activation and proliferation by inducing multiple growth factors or cytokines, such as PDGF, EGF, FGF, and TGF-β1 (Kilkenny *et al*., 2003; Choudhury *et al*., 2006; Skhirtladze *et al*., 2008).

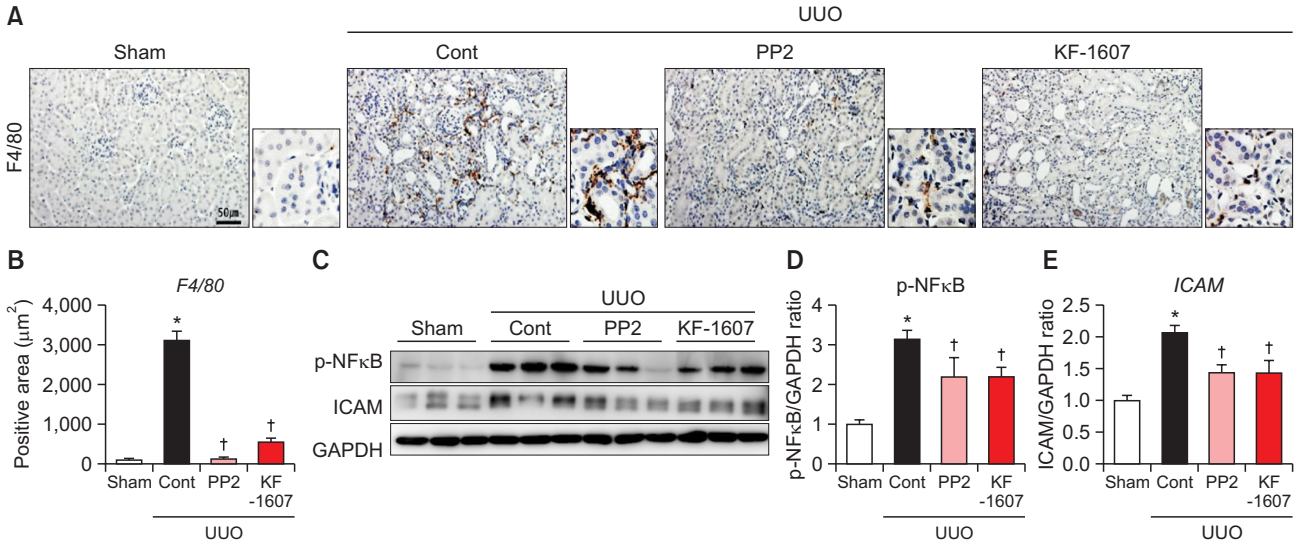

Fig. 7. Src kinase inhibition ameliorates kidney inflammation in UUO mice. Representative photomicrographs of (A) F4/80-stained kidney sections. The scale bar indicates 50 μm, original magnification x200. (B) Quantitative analysis of positively-stained areas in the cortex is depicted. (C) Protein expression of inflammation markers p-NFκB and ICAM were analyzed by immunoblotting. (D, E) Expression levels of the indicated proteins were quantified by densitometry and normalized with GAPDH. Values are presented as mean ± SE of 6 mice. **p*<0.05 vs. sham mice. †*p*<0.05 vs. UUO control mice.

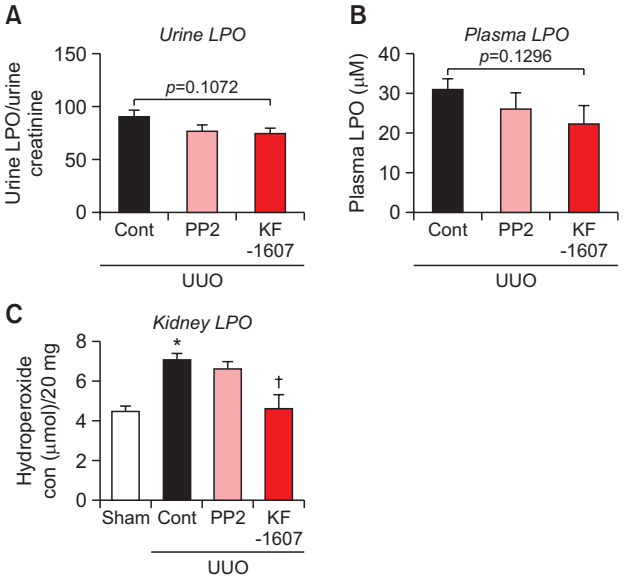

Fig. 8. Src kinase inhibition decreases oxidative stress in UUO kidney. LPO, a marker of oxidative stress, was analyzed in (A) urine, (B) plasma, and (C) kidney of experimental mice. Values are presented as mean ± SE of 6 mice. **p*<0.05 vs. sham mice. †*p*<0.05 vs. UUO control mice.

These mediators further stimulate renal fibroblast activation, and TGF-β1 is generally considered to be the most potent pro-fibrotic factor among them.

The present study demonstrated that a pan-Src kinase inhibitor with a new scaffold inhibited the activation of Fyn, Lyn, and Src kinases. This inhibition accordingly attenuated tubular injury and tubulointerstitial fibrosis to the same extent as PP2, a commonly used experimental SKI. Our findings were in parallel with previous studies with genetic modification and pharmacological treatment with other experimental SKIs. TGF-β1-induced renal interstitial fibroblast activation was attenuated by a SKI PP1 and Src siRNA. Src inhibition by PP1 also significantly ameliorated ECM deposition and pro-fibrotic signaling such as TGF-β1/Smad3, EGFR, and STAT3 (Yan *et al*., 2016). Recent findings suggest that Src serves as a direct Smad3 target gene and also contributes to macrophage-myofibroblast transition-driven kidney fibrosis (Tang *et al*., 2018). In another study, whole body Fyn knockout mice attenuated UUO-induced tubulointerstitial fibrosis, which was mainly dependent on inactivation of STAT3 but not the Smad signaling pathway (Seo *et al*., 2016).

As shown by its IC_{50s}, KF-1607 targets multiple SFKs members. Commercially available TKIs have been less studied in renal fibrosis animal models. Administration of dasatinib, a highly selective inhibitor of Hck, inhibited the progression of kidney fibrosis in mouse models of UUO, lupus nephritis, and folic acid nephropathy (Wei *et al*., 2016). Nintedanib inhibited the activation of Src, Lck, and Lyn kinases, as well as receptor type tyrosine kinases, i.e., PDGFR, FGFR, and VEGF which resulted in attenuation of inflammation and fibrotic development in obstructed kidneys (Liu *et al*., 2017). These results support the idea that pan molecule inhibitors which target several different signaling pathways may help to effectively inhibit fibrosis, a disease which involves diverse pathologic key events and activation. However, the clinical safety of a pan inhibitor is the most important issue to deal with (Beyer and Distler, 2013). Based on our current results from the *in vitro* cytotoxicity assay with renal mesangial cells, our new scaffold possesses relatively lower toxicity compared to ponatinib, a commercial TKI with potent cardiotoxicity. Still, specific cardiotoxicity studies are necessary to evaluate the compound's safety both in short and long administration periods.

Altogether, the present study suggested that multiple SFKs members are activated in response to UUO injury in mice. Pan-Src kinase inhibition by KF-1607, a next-generation TKI, significantly attenuated the progression of tubulointerstitial fibrosis in mice with UUO. Furthermore, this study is set as a precedent to further evaluate the role of SFK in mediating other CKDs, such as diabetic nephropathy, by utilizing the pan-Src kinase inhibitors. Comparing the efficacy of the pan-Src kinase inhibitors with a mainstay treatment of CKDs, such as renin-angiotensin system inhibitors, is a viable avenue of clinical investigation.

CONFLICT OF INTEREST

The authors have declared no conflict of interest.

ACKNOWLEDGMENTS

We thank Junghwa Lee for her excellent technical assistance. This work was supported by grants from the Korean Health Technology R&D Project through the Korean Health Industry Development Institute (HI18C0695).

REFERENCES

Beyer, C. and Distler, J. H. W. (2013) Tyrosine kinase signaling in fibrotic disorders: translation of basic research to human disease. *Biochim. Biophys. Acta* **1832**, 897-904.

Boggon, T. J. and Eck, M. J. (2004) Structure and regulation of Src family kinases. *Oncogene* **23**, 7918-7927.

Breyer, M. D. and Susztak, K. (2016) The next generation of therapeutics for chronic kidney disease. *Nat. Rev. Drug Discov.* **15**, 568-588.

Choudhury, G. G., Mahimainathan, L., Das, F., Venkatesan, B. and Ghosh-Choudhury, N. (2006) c-Src couples PI 3 kinase/Akt and MAPK signaling to PDGF-induced DNA synthesis in mesangial cells. *Cell. Signal.* **18**, 1854-1864.

De Nicola, L. and Zoccali, C. (2016) Chronic kidney disease prevalence in the general population: heterogeneity and concerns. *Nephrol. Dial. Transplant.* **31**, 331-335.

Drake, J. M., Lee, J. K. and Witte, O. N. (2014) Clinical targeting of mutated and wild-type protein tyrosine kinases in cancer. *Mol. Cell. Biol.* **34**, 1722-1732.

Flechner, S. M., Kurian, S. M., Head, S. R., Sharp, S. M., Whisenant, T. C., Zhang, J., Chismar, J. D., Horvath, S., Mondala, T., Gilmartin, T., Cook, D. J., Kay, S. A., Walker, J. R. and Salomon, D. R. (2004) Kidney transplant rejection and tissue injury by gene profiling of biopsies and peripheral blood lymphocytes. *Am. J. Transplant.* **4**, 1475-1489.

Gainor, J. F. and Chabner, B. A. (2015) Ponatinib: accelerated disapproval. *Oncologist* **20**, 847-848.

Ha, H., Yu, M. R. and Kim, K. H. (1999) Melatonin and taurine reduce early glomerulopathy in diabetic rats. *Free Radic. Biol. Med.* **26**, 944-950.

Hattori, S., Kanda, S. and Harita, Y. (2011) Tyrosine kinase signaling in kidney glomerular podocytes. *J. Signal Transduct.* **2011**, 317852.

Hill, N. R., Fatoba, S. T., Oke, J. L., Hirst, J. A., O'Callaghan, C. A., Lasserson, D. S. and Hobbs, F. D. (2016) Global prevalence of chronic kidney disease - a systematic review and meta-analysis. *PLoS ONE* **11**, e0158765.

Hu, M., Che, P., Han, X., Cai, G. Q., Liu, G., Antony, V., Luckhardt, T., Siegal, G. P., Zhou, Y., Liu, R. M., Desai, L. P., O'Reilly, P. J., Thannickal, V. J. and Ding, Q. (2014) Therapeutic targeting of Src kinase in myofibroblast differentiation and pulmonary fibrosis. *J. Pharmacol. Exp. Ther.* **351**, 87-95.

Kilkenny, D. M., Rocheleau, J. V., Price, J., Reich, M. B. and Miller, G. G. (2003) c-Src regulation of fibroblast growth factor-induced proliferation in murine embryonic fibroblasts. *J. Biol. Chem.* **278**, 17448-17454.

Lee, J., Hwang, I., Lee, J. H., Lee, H. W., Jeong, L. S. and Ha, H. (2013) The selective A3AR antagonist LJ-1888 ameliorates UUO-induced tubulointerstitial fibrosis. *Am. J. Pathol.* **183**, 1488-1497.

Liu, F., Wang, L., Qi, H., Wang, J., Wang, Y., Jiang, W., Xu, L., Liu, N. and Zhuang, S. (2017) Nintedanib, a triple tyrosine kinase inhibitor, attenuates renal fibrosis in chronic kidney disease. *Clin. Sci.* **131**, 2125-2143.

Lv, Z., Hu, M., Ren, X., Fan, M., Zhen, J., Chen, L., Lin, J., Ding, N., Wang, Q. and Wang, R. (2016) Fyn mediates high glucose-induced actin cytoskeleton reorganization of podocytes via promoting ROCK activation *in vitro*. *J. Diabetes Res.* **2016**, 5671803.

Meng, X. M., Tang, P. M. K., Li, J. and Lan, H. Y. (2015) TGF-ß/Smad signaling in renal fibrosis. *Front. Physiol.* **6**, 82.

Neusser, M. A., Lindenmeyer, M. T., Moll, A. G., Segerer, S., Edenhofer, I., Sen, K., Stiehl, D. P., Kretzler, M., Gröne, H. J., Schlöndorff, D. and Cohen, C. D. (2010) Human nephrosclerosis triggers a hypoxia-related glomerulopathy. *Am. J. Pathol.* **176**, 594-607.

O'Hare, T., Shakespeare, W. C., Zhu, X., Eide, C. A., Rivera, V. M., Wang, F., Adrian, L. T., Zhou, T., Huang, W. S., Xu, Q., Metcalf, C. A., 3rd, Tyner, J. W., Loriaux, M. M., Corbin, A. S., Wardwell, S., Ning, Y., Keats, J. A., Wang, Y., Sundaramoorthi, R., Thomas, M., Zhou, D., Snodgrass, J., Commodore, L., Sawyer, T. K., Dalgarno, D. C., Deininger, M. W., Druker, B. J. and Clackson, T. (2009) AP24534, a pan-BCR-ABL inhibitor for chronic myeloid leukemia, potently inhibits the T315I mutant and overcomes mutation-based resistance. *Cancer Cell* **16**, 401-412.

Papadopoulos, T., Krochmal, M., Cisek, K., Fernandes, M., Husi, H., Stevens, R., Bascands, J. L., Schanstra, J. P. and Klein, J. (2016) Omics databases on kidney disease: where they can be found and how to benefit from them. *Clin. Kidney J.* **9**, 343-352.

Papatheodorou, I., Fonseca, N. A., Keays, M., Tang, Y. A., Barrera, E., Bazant, W., Burke, M., Füllgrabe, A., Fuentes, A. M., George, N., Huerta, L., Koskinen, S., Mohammed, S., Geniza, M., Preece, J., Jaiswal, P., Jarnuczak, A. F., Huber, W., Stegle, O., Vizcaino, J. A., Brazma, A. and Petryszak, R. (2018) Expression Atlas: gene and protein expression across multiple studies and organisms. *Nucleic Acids Res.* **46**, D246-D251.

Parsons, S. J. and Parsons, J. T. (2004) Src family kinases, key regulators of signal transduction. *Oncogene* **23**, 7906-7909.

Ruggenenti, P., Cravedi, P. and Remuzzi, G. (2012) Mechanisms and treatment of CKD. *J. Am. Soc. Nephrol.* **23**, 1917-1928.

Seo, H. Y., Jeon, J. H., Jung, Y. A., Jung, G. S., Lee, E. J., Choi, Y. K., Park, K. G., Choe, M. S., Jang, B. K., Kim, M. K. and Lee, I. K. (2016) Fyn deficiency attenuates renal fibrosis by inhibition of phospho-STAT3. *Kidney Int.* **90**, 1285-1297.

Skhirtladze, C., Distler, O., Dees, C., Akhmetshina, A., Busch, N., Venalis, P., Zwerina, J., Spriewald, B., Pileckyte, M., Schett, G. and Distler, J. H. (2008) Src kinases in systemic sclerosis: central roles in fibroblast activation and in skin fibrosis. *Arthritis Rheum.* **58**, 1475-1484.

Sureshbabu, A., Muhsin, S. A. and Choi, M. E. (2016) TGF-β signaling in the kidney: profibrotic and protective effects. *Am. J. Physiol. Renal Physiol.* **310**, F596-F606.

Tang, P. M. K., Zhou, S., Li, C. J., Liao, J., Xiao, J., Wang, Q. M., Lian, G. Y., Li, J., Huang, X. R., To, K. F., Ng, C. F., Chong, C. C., Ma, R. C., Lee, T. L. and Lan, H. Y. (2018) The proto-oncogene tyrosine protein kinase Src is essential for macrophage-myofibroblast transition during renal scarring. *Kidney Int.* **93**, 173-187.

Taniguchi, K., Xia, L., Goldberg, H. J., Lee, K. W. K., Shah, A., Stavar, L., Masson, E. A., Momen, A., Shikatani, E. A., John, R., Husain, M. and Fantus, I. G. (2013) Inhibition of src kinase blocks high glucose-induced EGFR transactivation and collagen synthesis in mesangial cells and prevents diabetic nephropathy in mice. *Diabetes* **62**, 3874-3886.

Thomas, S. M. and Brugge, J. S. (1997) Cellular functions regulated by Src family kinases. *Annu. Rev. Cell Dev. Biol.* **13**, 513-609.

Wei, C., Li, L., Menon, M. C., Zhang, W., Fu, J., Kidd, B., Keung, K.

L., Woytovich, C., Greene, I., Xiao, W., Salem, F., Yi, Z., He, J. C., Dudley, J. T. and Murphy, B. (2016) Genomic analysis of kidney allograft injury identifies hematopoietic cell kinase as a key driver of renal fibrosis. *J. Am. Soc. Nephrol.* **28**, 1385-1393.

Wu, H., Shi, Y., Deng, X., Su, Y., Du, C., Wei, J., Ren, Y., Wu, M., Hou, Y. and Duan, H. (2015) Inhibition of c-Src/p38 MAPK pathway ameliorates renal tubular epithelial cells apoptosis in db/db mice. *Mol. Cell. Endocrinol.* **417**, 27-35.

Wynn, T. A. and Ramalingam, T. R. (2012) Mechanisms of fibrosis: Therapeutic translation for fibrotic disease. *Nat. Med.* **18**, 1028-1040.

Xiong, C., Zang, X., Zhou, X., Liu, L., Masucci, M. V., Tang, J., Li, X., Liu, N., Bayliss, G., Zhao, T. C. and Zhuang, S. (2017) Pharmacological inhibition of Src kinase protects against acute kidney injury in a murine model of renal ischemia/reperfusion. *Oncotarget* **8**, 31238-31253.

Yan, Y., Ma, L., Zhou, X., Ponnusamy, M., Tang, J., Zhuang, M. A., Tolbert, E., Bayliss, G., Bai, J. and Zhuang, S. (2016) Src inhibition blocks renal interstitial fibroblast activation and ameliorates renal fibrosis. *Kidney Int.* **89**, 68-81.

Zhou, D. and Liu, Y. (2016a) Renal fibrosis in 2015: understanding the mechanisms of kidney fibrosis. *Nat. Rev. Nephrol.* **12**, 68-70.

Zhou, D. and Liu, Y. (2016b) Therapy for kidney fibrosis: is the Src kinase a potential target? *Kidney Int.* **89**, 12-14.